

*The following article has been submitted to Applied Physics Letters (APL).
After it is published, it will be found at <https://pubs.aip.org/aip/apl>*

Thermal stability and phase transformation of α -, $\kappa(\epsilon)$ -, and γ - Ga_2O_3 thin films to β - Ga_2O_3 under various ambient conditions

Jingyu Tang,^{1,a)} Kunyao Jiang,¹ Po-Sen Tseng,¹ Rachel C. Kurchin,¹ Lisa M. Porter,¹ and Robert F. Davis^{1,2}

Affiliations

¹Department of Materials Science and Engineering, Carnegie Mellon University, Pittsburgh, Pennsylvania 15213, USA

²Department of Electrical and Computer Engineering, Carnegie Mellon University, Pittsburgh, Pennsylvania 15213, USA

^{a)}Author to whom correspondence should be addressed: jingyuta@andrew.cmu.edu

Abstract

Phase transitions in metastable α -, $\kappa(\epsilon)$ -, and γ - Ga_2O_3 films to thermodynamically stable β - Ga_2O_3 during annealing in air, N_2 , and vacuum have been systematically investigated via in-situ high-temperature X-ray diffraction (HT-XRD) and scanning electron microscopy (SEM). These respective polymorphs exhibited thermal stability to ~ 471 - 525°C , ~ 773 - 825°C , and ~ 490 - 575°C before transforming into β - Ga_2O_3 , across all tested ambient conditions. Particular crystallographic orientation relationships were observed before and after the phase transitions, i.e. (0006) α - $\text{Ga}_2\text{O}_3 \rightarrow (\bar{4}02)$ β - Ga_2O_3 , (004) $\kappa(\epsilon)$ - $\text{Ga}_2\text{O}_3 \rightarrow (310)$ and $(\bar{4}02)$ β - Ga_2O_3 , and (400) γ - $\text{Ga}_2\text{O}_3 \rightarrow (400)$ β - Ga_2O_3 . The phase transition of α - Ga_2O_3 to β - Ga_2O_3 resulted in catastrophic damage to the film and upheaval of the surface. The respective primary and possibly secondary causes of this damage are the +8.6% volume expansion and the dual displacive and reconstructive transformations that occur during this transition. The $\kappa(\epsilon)$ - and γ - Ga_2O_3 films converted to β - Ga_2O_3 via singular reconstructive transformations with small changes in volume and unchanged surface microstructures.

Gallium oxide (Ga_2O_3) occurs in four universally accepted polymorphs: α -(trigonal), β -(monoclinic), γ -(cubic-defective spinel), and $\kappa(\epsilon)$ -(orthorhombic) Ga_2O_3 . The existence of a fifth polymorph, δ - Ga_2O_3 , with a cubic-bixbyite structure remains under debate.¹ Among these polymorphs, β - Ga_2O_3 is the thermodynamically stable phase to its melting point; all other polymorphs convert to β - Ga_2O_3 when heated.² While β - Ga_2O_3 has attracted the most attention for its potential in high-power electronics and optoelectronics applications, the monoclinic symmetry of this polymorph creates anisotropy in its optical, electronic, and thermal properties.³⁻⁶ As such, the metastable polymorphs with their distinct crystal structures, symmetries, and properties have recently garnered considerable interest.

α - Ga_2O_3 has the largest bandgap (~ 5.3 eV^{7,8}) among all the polymorphs and is a promising alternative material for applications in high-power electronics, as indicated by its higher Baliga figure of merit relative to β - Ga_2O_3 .⁹ Electrical measurements of Schottky barrier diodes fabricated on α - Ga_2O_3 have shown a lower on-resistance of ~ 0.1 m $\Omega\cdot\text{cm}^2$ (Ref. 10) compared with > 2 m $\Omega\cdot\text{cm}^2$ for β - Ga_2O_3 .^{11,12} α - $\text{In}_2\text{O}_3/\alpha$ - Ga_2O_3 p-n junctions have also been reported.^{13,14} Moreover, the bandgap of α - Ga_2O_3 can be tuned via alloying with other oxides such as Al_2O_3 and In_2O_3 .^{9,15}

that possess the same corundum structure. $\kappa(\epsilon)$ -Ga₂O₃ is also of considerable interest as it is the only polymorph that lacks inversion symmetry, meaning that spontaneous polarization is theoretically possible and this material could be piezoelectric (and possibly ferroelectric).^{16,17} If ferroelectricity were to occur in $\kappa(\epsilon)$ -Ga₂O₃, the magnitude has been predicted to be an order of magnitude higher than in AlN and GaN.^{18,19} Prior work on γ -Ga₂O₃ has indicated its potential utility in applications such as photoluminescence, catalytic and photocatalytic degradation of select organic compounds, and room-temperature ferromagnetism when incorporated with Mn.^{20–22} For these and other applications, it is crucial to understand maximum operating temperatures for these metastable polymorphs, as well as the upper limits of the post-fabrication thermal treatments such as rapid thermal annealing of metal contacts and post-annealing after ion implantation for dopant activation.

Several studies have examined the thermal stability of α - and $\kappa(\epsilon)$ -Ga₂O₃ across varying film thicknesses and annealing processes, including both ex-situ and in-situ methods along with different ramping/cooling rates and holding periods at specific temperatures.^{23–27} In this Letter, a comprehensive analysis of the thermal stability of α -, $\kappa(\epsilon)$ -, and γ -Ga₂O₃ epitaxial films, maintained at a similar thickness and subjected to an identical in-situ annealing sequence, was undertaken under three ambient conditions. The effect of the annealing environment on thermal stability and the evolution of surface morphologies are detailed for each polymorph.

The epitaxial films investigated in this Letter were α -Ga₂O₃ grown on (0001) sapphire via halide vapor phase epitaxy (HVPE) by Kyma Technologies, and $\kappa(\epsilon)$ - and γ -Ga₂O₃ grown on (0001) sapphire and (100) MgAl₂O₄ (spinel) substrates, respectively, via vertical, low-pressure, cold-wall metal-organic chemical vapor deposition (MOCVD). The details regarding the precursors and parameters employed for the growth of our $\kappa(\epsilon)$ - and γ -Ga₂O₃ films have been reported in previous publications.^{28,29} High-resolution X-ray diffraction (HR-XRD) patterns of the as-grown films were acquired using a Panalytical X'pert Pro MPD X-ray diffractometer having a 4-crystal Ge \times (220) monochromator. HT-XRD patterns were recorded with a Malvern Panalytical Empyrean diffractometer (mirror optics) equipped with a HTK 16N high-temperature chamber that can be heated to 1600°C. The latter equipment was employed to observe phase transitions in our metastable polymorphs to β -Ga₂O₃ as a function of temperature in air, ultra-high purity (5N) N₂ and vacuum ($\sim 5 \times 10^{-5}$ Torr). Each Ga₂O₃ film/substrate assembly was heated in increments of 100°C and held at each temperature for 1 hr while the XRD data were acquired. Heating in increments of 25°C was applied near the phase transition temperature to observe the dynamics of this transition in each metastable polymorph. The ramping rate was set at 30°C/min to 500°C and reduced to 10°C/min for higher temperatures. The cooling rate was set to be 30°C/min. Before initiating in-situ measurements in N₂, the HT-XRD chamber underwent five pump-and-purge cycles to ensure the elimination of residual gases. As discussed below, temperature calibration under vacuum was necessary after the measurement due to the changes in the modes of heating in this environment. Scanning electron microscopy (SEM) was performed to investigate the evolution of the surface morphology of the as-grown and post-annealed films for each polymorph.

Figures 1(a)-1(c) show 2θ - ω scans of α -Ga₂O₃, $\kappa(\epsilon)$ -Ga₂O₃, and γ -Ga₂O₃ films grown on c-plane sapphire, c-plane sapphire, and (100) MgAl₂O₄, respectively. Figure 1(b) reveals a shoulder near the (004) $\kappa(\epsilon)$ -Ga₂O₃ peak, attributed to the presence of ($\bar{4}02$) β -Ga₂O₃ within the film, a common observation for $\kappa(\epsilon)$ -Ga₂O₃ films grown by MOCVD.^{28,30,31} β -Ga₂O₃ has been shown to be present near the film-substrate interface.^{28,31} Jinno et al.²⁴ reported a strong correlation between

film thickness and thermal stability of α -Ga₂O₃ films deposited on c-plane sapphire; the thinner the film, the more stable upon heat treatment. To mitigate thickness and substrate-induced strain effects on thermal stability of our films, the thicknesses were maintained at $\sim 0.9\mu\text{m}$ and confirmed to be in a relaxed state in reciprocal space maps (RSMs) shown in Figs. 1(d)-1(f). The separation of the vertical line passing through the center of the film spot (black dashed line) and substrate spot (red dashed line) indicates that these films were in a relaxed state.

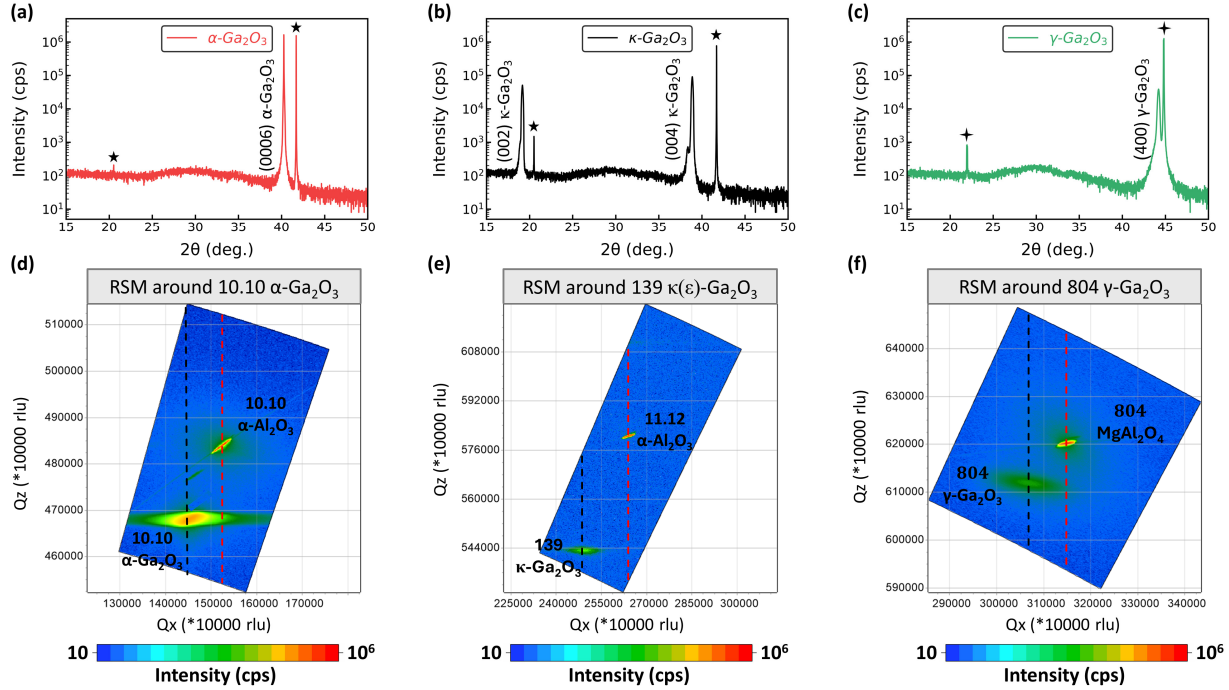


Figure 1: High-resolution 2θ - ω scans displayed on a log scale for (a) α -Ga₂O₃ on c-sapphire, (b) $\kappa(\epsilon)$ -Ga₂O₃ on c-sapphire, and (c) γ -Ga₂O₃ on (100) MgAl₂O₄ as-grown films, and their associated RSMs in (d)-(f). The starred peaks in the X-ray patterns are from the respective substrates.

Figure 2(a) shows the in-situ HT-XRD patterns of α -Ga₂O₃ annealed in air in the temperature range from 500°C to 900°C. These patterns reveal that (0001) oriented α -Ga₂O₃ maintains its thermal stability to 525°C. However, a phase transition is initiated at $\sim 550^\circ\text{C}$, which results in the formation of ($\bar{2}01$) oriented β -Ga₂O₃. The results of six consecutive scans for 10min each conducted over 1 hr annealing periods at both 525°C and 550°C are illustrated in Figs. 2(a1) and 2(a2), respectively. Notably, the α -Ga₂O₃ film annealed at 525°C exhibits no detectable phase change, as evidenced by the nearly constant intensity of the (0006) α -Ga₂O₃ peak, depicted in Fig. 2(a1). In contrast, Figure 2(a2) reveals a noticeable decrease in the intensity of the (0006) α -Ga₂O₃ peak accompanied by a gradual increase in the intensity of the ($\bar{4}02$) β -Ga₂O₃ peak for the film annealed at 550°C. The α -Ga₂O₃ film is completely converted to β -Ga₂O₃ after annealing at 600°C, because the α -Ga₂O₃ peak is no longer detectable and further increases in temperature do not affect the peak intensity of ($\bar{4}02$) β -Ga₂O₃. Wen et al.²³ determined using in-situ HT-XRD that a 4 μm thick α -Ga₂O₃ grown on c-plane sapphire by HVPE was thermally stable up to 500-540 °C in air. Studies by other investigators^{24,25} also demonstrated enhanced thermal stability of α -Ga₂O₃ beyond 600°C via reduction of the film thickness to ~ 100 nm on c- and m-plane sapphire. Furthermore,

they determined that either the application of the selective area growth method to release the strain within the film²⁴ or the deposition of an AlO_x capping layer to suppress the decomposition in tandem with the application of strain to the film²⁵ further extended the thermal stability of α -Ga₂O₃ to within the temperature range of 800-900°C.

Figure 2(b) presents the in-situ HT-XRD patterns of $\kappa(\epsilon)$ -Ga₂O₃ annealed in air in the same temperature range from 500°C to 900°C. The (001) oriented $\kappa(\epsilon)$ -Ga₂O₃ was thermally stable to 800°C, with a phase transition to both ($\bar{4}$ 02) and (310) oriented β -Ga₂O₃ starting around 825°C. This transition is detailed in the six successive scans over a 1 hr annealing period at both 825°C and 850°C, as shown in Figs. 2(b1) and 2(b2), respectively. Annealing at 825°C resulted in a gradual decrease in the intensity of the (004) $\kappa(\epsilon)$ -Ga₂O₃ peak and an increase in the intensity of both ($\bar{4}$ 02) and (310) β -Ga₂O₃ peaks towards the end of the 1 hr annealing period, as shown in Fig. 2(b1). The transition occurred more rapidly for the film annealed at 850°C (Fig. 2(b2)). $\kappa(\epsilon)$ -Ga₂O₃ was completely converted to β -Ga₂O₃, as there was no detectable $\kappa(\epsilon)$ -Ga₂O₃ peak and no discernible increase in the peak intensity of either the ($\bar{4}$ 02) or the (310) β -Ga₂O₃ peaks when the temperature exceeded 850°C. The coexistence of ($\bar{4}$ 02) and (310) β -Ga₂O₃ may be attributed to their similar oxygen sublattice atomic arrangements and lattice mismatches with (0001) α -Ga₂O₃. Studies by Fornari et al.²⁶ revealed that cooling $\kappa(\epsilon)$ -Ga₂O₃ films from 1000°C at a rate of 7.5°C/min and 2°C/min resulted in the evolution of either the (310) or ($\bar{4}$ 02) peak, respectively, as the dominant β -Ga₂O₃ peak. Recently, Xu et al.³² explored the competitive growth of the (310) and the ($\bar{4}$ 02) orientations of β -Ga₂O₃ grown on c-plane sapphire by HVPE. They noted the similarity of the atomic arrangements of these two planes and the c-plane of sapphire, and the effect of growth temperatures and HCl flow rates on the formation of the energetically unfavorable (310) oriented β -Ga₂O₃.

Figure 2(c) presents the in-situ HT-XRD patterns of γ -Ga₂O₃ annealed in air within the aforementioned temperature range. The (100) oriented γ -Ga₂O₃ was determined to be thermally stable to 575°C; however, a phase transition to (100) oriented β -Ga₂O₃ was initiated at ~600 °C. This transition progressed more slowly than those observed for α - and $\kappa(\epsilon)$ -Ga₂O₃. Successive scans over 1 hr annealing periods at 575°C and 900°C are shown in Figs. 2(c1) and 2(c2), respectively. The scans in Figure 2(c1) exhibit no significant phase change, as evidenced by the nearly constant intensity of the (400) γ -Ga₂O₃ peak. The small lattice mismatch (~+1.9%) between the γ -Ga₂O₃ film and the MgAl₂O₄ substrate, combined with the resolution limits of the XRD equipment, made difficult the observation of the (400) γ -Ga₂O₃ peak below 3600 cps, since the background intensity at the same 2θ position for a bare MgAl₂O₄ substrate is approximately 3600 cps. Thus, the continued increase of the (400) β -Ga₂O₃ peak for the film annealed at 900°C suggests an incomplete phase transition, as shown in Fig. 2(c2). Further increasing the annealing temperature to 1000°C caused significant Mg and Al interatomic diffusion from the substrate into the film and resulted in the formation of γ -Ga₂O₃ solid solutions, as detailed in our earlier publications.^{33,34}

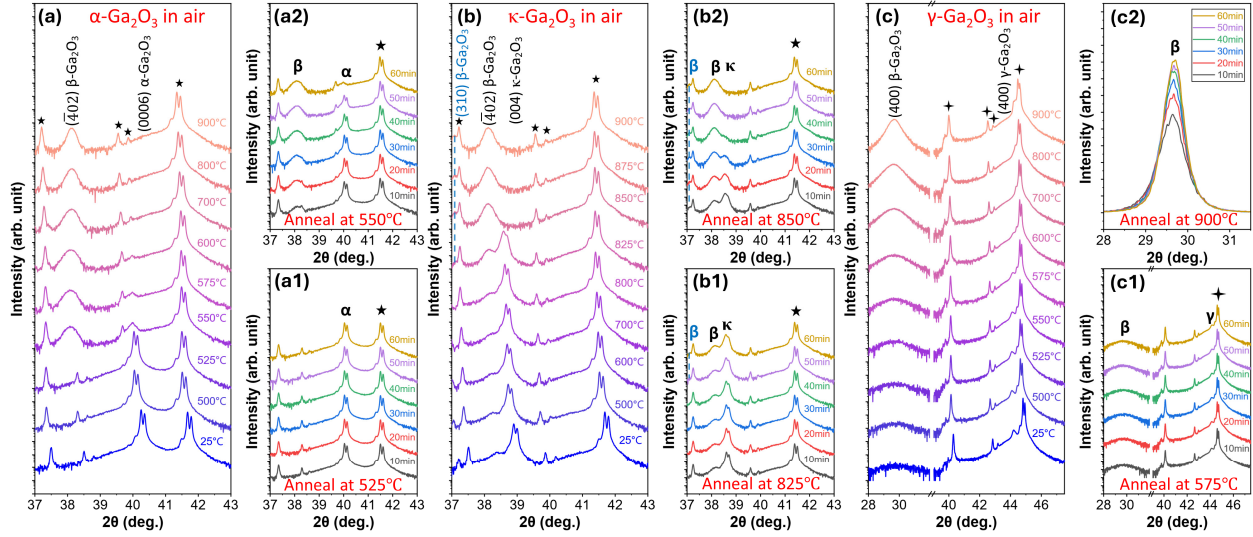


Figure 2: HT-XRD 2θ - ω scans conducted in air for (a) α - Ga_2O_3 on c-sapphire, (b) $\kappa(\epsilon)$ - Ga_2O_3 on c-sapphire, and (c) γ - Ga_2O_3 on (100) MgAl_2O_4 , respectively, in the temperature range of 500-900°C. The starred peaks in the X-ray patterns are from the respective substrates.

Figures 3(a)-3(c) show the in-situ HT-XRD patterns of α - Ga_2O_3 , $\kappa(\epsilon)$ - Ga_2O_3 and γ - Ga_2O_3 films, respectively, annealed in N_2 within the temperature range of 500°C to 900°C. Similar to the observations made in air, the α - Ga_2O_3 , $\kappa(\epsilon)$ - Ga_2O_3 and γ - Ga_2O_3 films were thermally stable to approximately 525°C, 825°C, and 575°C, respectively. Almost no detectable decrease in the film peak intensities occurred during the 1 hr annealing period at these temperatures, as shown in Figs. 3(a1), 3(b1) and 3(c1). Lee et al.²⁷ reported that an α - Ga_2O_3 film with a thickness of $\sim 720\text{nm}$ was thermally stable to 550°C in N_2 . Fornari et al.²⁶ determined via ex-situ annealing that phase transitions in 500nm thick $\kappa(\epsilon)$ - Ga_2O_3 films occurred around 900°C, in both O_2 and N_2 atmospheres.

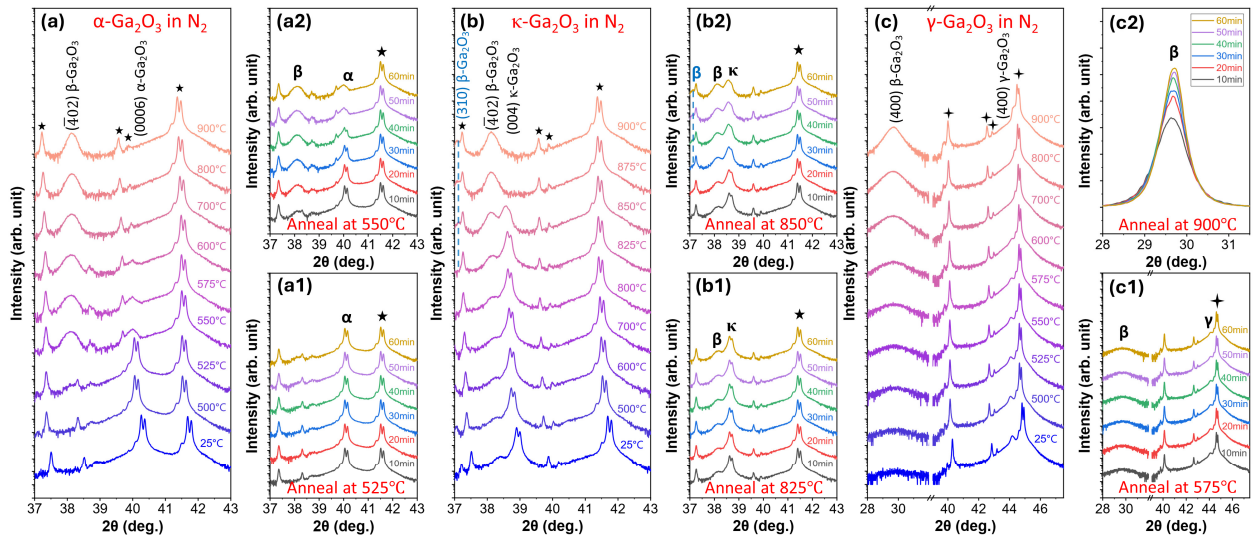


Figure 3: HT-XRD 2θ - ω scans conducted in N_2 for (a) α - Ga_2O_3 on c-sapphire, (b) $\kappa(\epsilon)$ - Ga_2O_3 on c-sapphire, and (c) γ - Ga_2O_3 on (100) $MgAl_2O_4$, respectively, in the temperature range of 500-900°C. The starred peaks in the X-ray patterns are from the respective substrates.

The in-situ HT-XRD experiments under vacuum were conducted with the sample temperature range from 110°C to 865°C based on the calibration process described below. The temperature difference between the platinum stage and the surface of the sapphire and spinel substrates was determined to be less than 20°C when the stage temperature was below 900°C in air and N_2 . However, in conducting the same in-situ measurements in vacuum, significant temperature differences were noted between the sample stage and the substrate because of the poor heat transfer in vacuum, likely due to lack of convection to the sample surface from the atmosphere. This observation was initially identified from the inconsistency in the calculated out-of-plane lattice constants of the sapphire and spinel substrates beneath the α - Ga_2O_3 , $\kappa(\epsilon)$ - Ga_2O_3 , and γ - Ga_2O_3 films, in comparison to similar data acquired for these substrates heated in air and N_2 , as shown in Figs. 4(a)-4(c). Temperature calibration in vacuum was done based on the second-order polynomial fit of the out-of-plane lattice vs. temperature determined in air and N_2 . Figures 4(d)-4(f) show a consistent out-of-plane lattice constant of the sapphire and spinel substrates versus calibrated temperature.

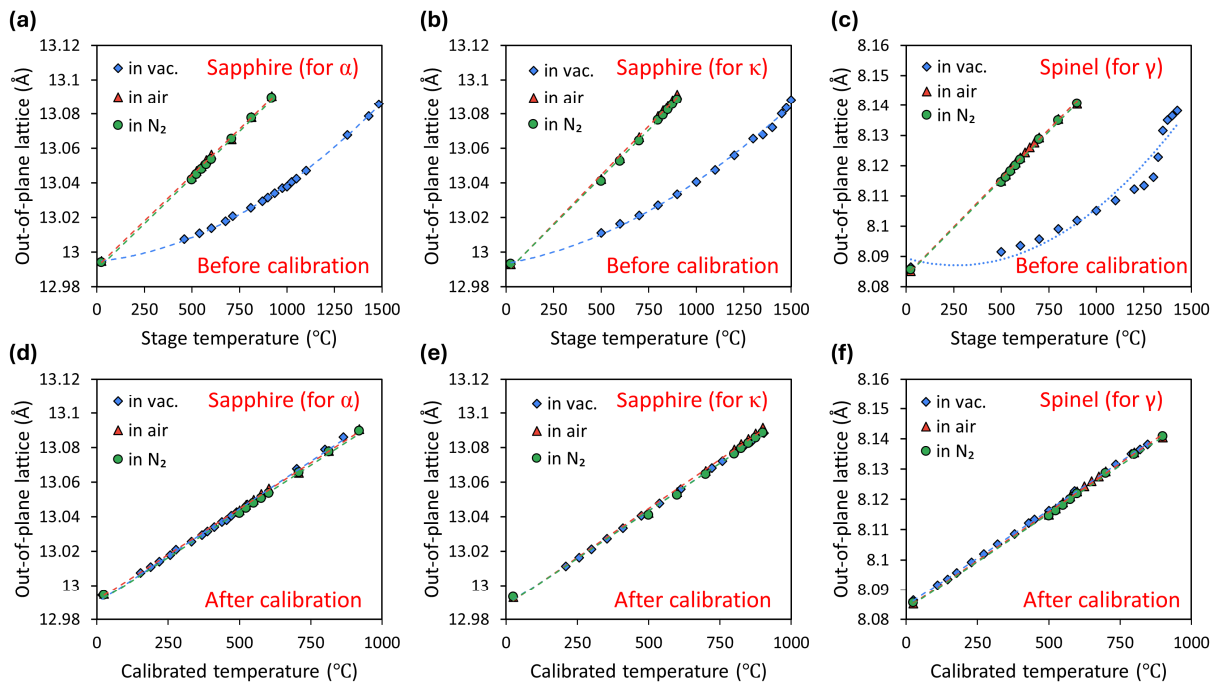


Figure 4: Out-of-plane lattice constants versus stage or calibrated temperature for sapphire and spinel substrates in vacuum before and after calibration.

Figures 5(a)-5(c) present the in-situ HT-XRD patterns of α - Ga_2O_3 , $\kappa(\epsilon)$ - Ga_2O_3 , and γ - Ga_2O_3 films annealed in vacuum from room temperature to $\sim 900^\circ C$. Consistent with findings in air and N_2 , the thermal stabilities of α - Ga_2O_3 , $\kappa(\epsilon)$ - Ga_2O_3 and γ - Ga_2O_3 films were maintained within the ranges of 471-490°C, 773-818°C, and 490-590°C, respectively, as shown in Figs. 5(a1), 5(b1) and 5(c1). As noted above, Wen et al.²³ conducted a similar HT-XRD study on α - Ga_2O_3 films grown

on c-sapphire substrates and annealed within the temperature range of under a vacuum of 10^{-4} Torr. They observed that the phase transition to β - Ga_2O_3 occurred at 700°C , a temperature 200°C higher than annealing in air. This variation is thought to be attributed to the difference in oxygen partial pressures affecting oxygen diffusion. They surmised that the oxygen concentrations of the various intermediate GaO_x compositions decrease during the transformation with the decrease in $p\text{O}_2$ due to the reduction of oxygen diffusion. This phenomenon eventually increases the overall kinetic barrier for phase transformation. However, our results did not indicate a similar enhancement in thermal stability under vacuum in any of the three metastable polymorphs. We hypothesize that this may be related to the length of time the samples were held at each temperature. Wen et al. stabilized the sample for 5 min at each temperature before recording the data; we held the sample for 1 hr, during which six successive scans were performed to verify whether the system had reached equilibrium.

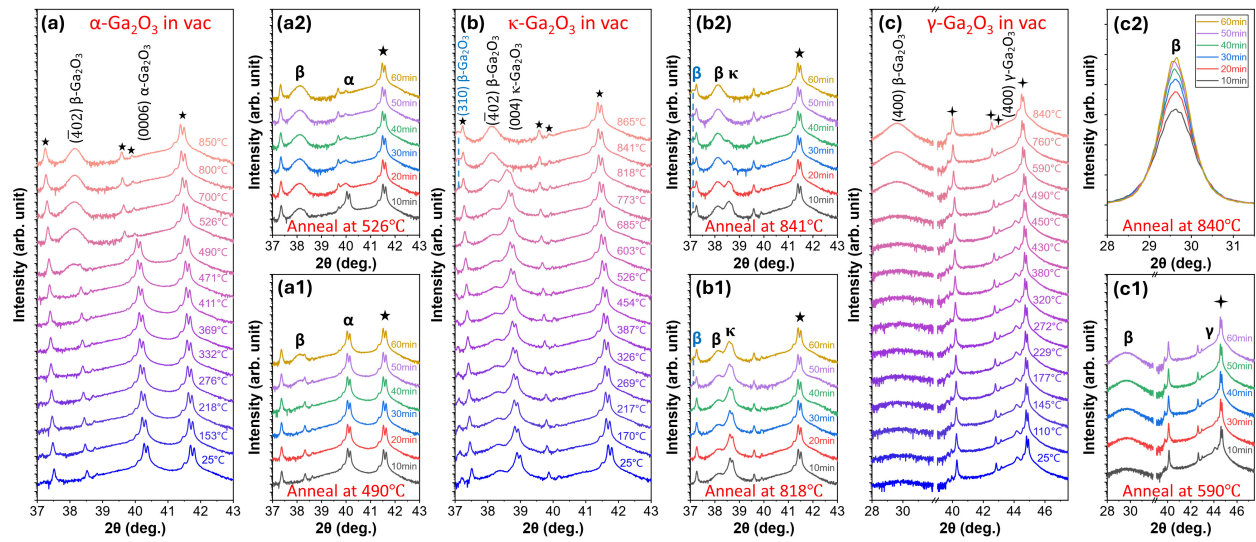


Figure 5: HT-XRD 2θ - ω scans conducted in vacuum with a base pressure of 5×10^{-5} Torr for (a) α - Ga_2O_3 on c-sapphire, (b) $\kappa(\epsilon)$ - Ga_2O_3 on c-sapphire, and (c) γ - Ga_2O_3 on (100) MgAl_2O_4 , respectively, in the calibrated temperature range of 110 – 865°C . The starred peaks in the X-ray patterns are from the respective substrates.

Figure 6 displays the SEM images of both as-grown and post-annealed α - Ga_2O_3 , $\kappa(\epsilon)$ - Ga_2O_3 , and γ - Ga_2O_3 films processed under various conditions. As detailed above, annealing the films resulted in their complete phase transformation into β - Ga_2O_3 . Only the α - Ga_2O_3 films experienced a catastrophic phase transition characterized by widespread rupture and upheaval of the surface across the entire material regardless of the ambient conditions. A similar observation has been reported in α - Ga_2O_3 films by Wen et al.²³ This phenomenon of marked film damage is similar to that observed during the θ -alumina ($C2/m$, structurally equivalent to β - Ga_2O_3) to α -alumina ($R\bar{3}c$, structurally equivalent to α - Ga_2O_3) phase transition. This latter transition has been attributed to a substantial volume reduction of ~ 10 vol%^{35,36} during heating. In the case of the α - to β - Ga_2O_3 transition, a positive volume expansion of $+8.6$ vol% is involved and is the primary cause of the severe film damage. In contrast, the $\kappa(\epsilon)$ - Ga_2O_3 and γ - Ga_2O_3 films maintained their surface morphologies after each phase transition in the three ambient conditions. The data presented in Table I provide a comparison of the change in volume of each metastable Ga_2O_3 phase in relation

to β -Ga₂O₃ as well as the type of phase transition, density, and the oxygen sublattice arrangement in each phase. The transformation of α -Ga₂O₃ to β -Ga₂O₃ is both a displacive and a reconstructive phase transition, which is likely a secondary cause of the disruption in the microstructure. The shearing of the oxygen sublattice from hexagonal close-packing (HCP) to face-centered cubic (FCC) packing is classified as a diffusionless displacive (martensitic) transition.³⁷ However, the relocation of gallium cations involves short-range diffusion and synchronized shear with the oxygen sublattice and is classified as a reconstructive transition.³⁷ By comparison, the oxygen sublattices for $\kappa(\epsilon)$ -Ga₂O₃ and γ -Ga₂O₃ are FCC structures, which are structurally similar to the oxygen sublattice in β -Ga₂O₃. The phase transitions in these two polymorphs primarily involve short-range diffusion and are thus reconstructive transitions. Theoretical studies on the transition from γ -Al₂O₃ (Fd $\bar{3}$ m, structurally equivalent to γ -Ga₂O₃) to θ -alumina suggest it involves local migration of Al atoms without the shearing of the oxygen sublattice.³⁸ The volume changes associated with the phase transitions in $\kappa(\epsilon)$ -Ga₂O₃ and γ -Ga₂O₃ are much smaller than that in α -Ga₂O₃, as shown in Table I, and contribute markedly to the preservation of the surface morphology during the phase transition in each polymorph.

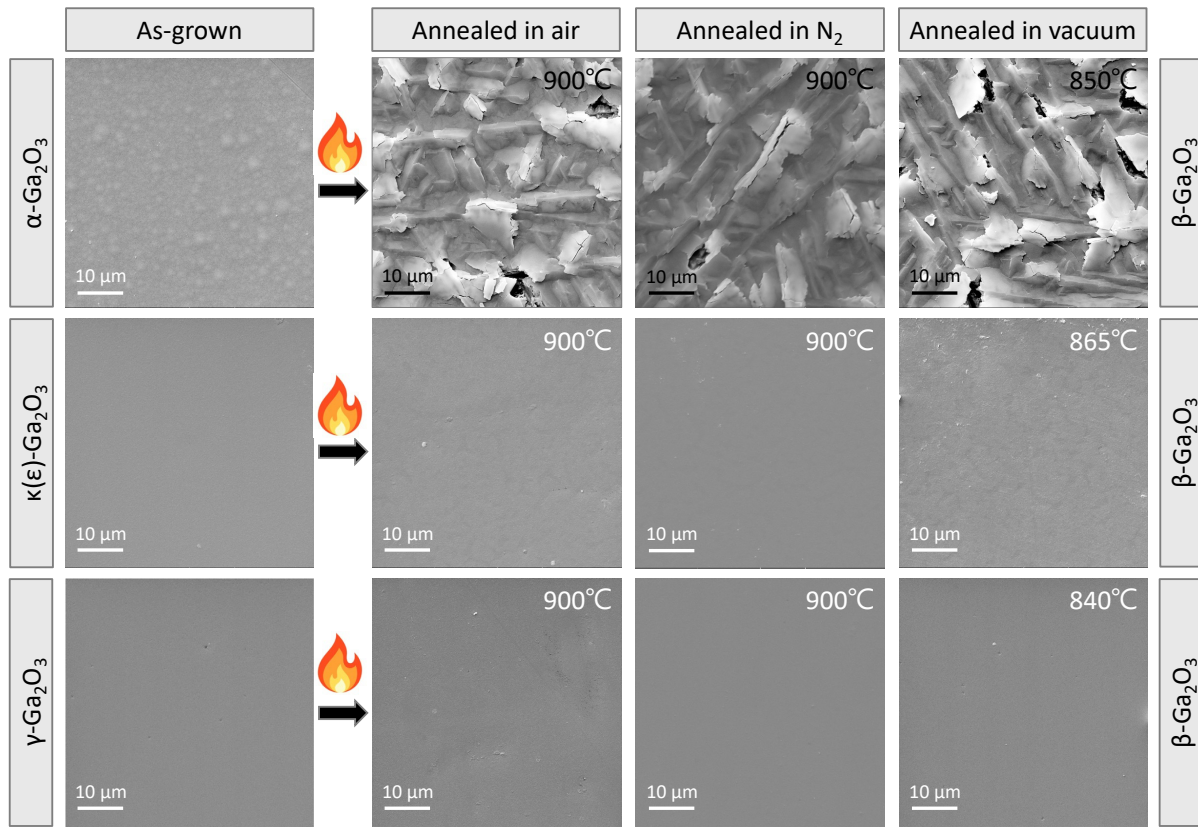


Figure 6: SEM images of the α -Ga₂O₃, $\kappa(\epsilon)$ -Ga₂O₃, and γ -Ga₂O₃ films before and after annealing under different ambient conditions. All films converted to β -Ga₂O₃ by \sim 900°C.

Table I. Comparison of the density, change in volume at room temperature, and type of phase transition involved in the transformation of α -Ga₂O₃, $\kappa(\epsilon)$ -Ga₂O₃, and γ -Ga₂O₃ films to β -Ga₂O₃.

Phase	Density (g/cm ³)	Δ volume with respect to β (%)	O sublattice atomic arrangement	Phase transition type
α -Ga ₂ O ₃	$\sim 6.453^{39,40}$	+8.6	HCP	displacive + reconstructive ³⁷
$\kappa(\epsilon)$ -Ga ₂ O ₃	$\sim 6.111^{41,42}$	+2.8	FCC	reconstructive
γ -Ga ₂ O ₃	$\sim 5.940^{41,43}$	-0.05	FCC	reconstructive
β -Ga ₂ O ₃	$\sim 5.943^{44,45}$	0	FCC	-

The thermal stability and phase evolution of structurally relaxed, $\sim 1\mu\text{m}$ thick films of α -Ga₂O₃, $\kappa(\epsilon)$ -Ga₂O₃, and γ -Ga₂O₃ have been determined via in-situ HT-XRD in air, N₂, and vacuum environments. These polymorphs exhibited stability against transformation to β -Ga₂O₃ up to ~ 471 - 525°C , ~ 773 - 825°C , and ~ 490 - 575°C , respectively, across all tested ambient conditions. Strong crystallographic orientation relationships were observed before and after the phase transitions, namely, (0006) α -Ga₂O₃ \rightarrow ($\bar{4}02$) β -Ga₂O₃, (004) $\kappa(\epsilon)$ -Ga₂O₃ \rightarrow (310) and ($\bar{4}02$) β -Ga₂O₃, and (400) γ -Ga₂O₃ \rightarrow (400) β -Ga₂O₃. Notably, the α -Ga₂O₃ film experienced a catastrophic transformation characterized by severe rupture and upheaval of the surface under all ambient conditions and primarily caused by the significant positive volume expansion during the transition. The changes in the arrangement of oxygen and gallium sublattices during the α -Ga₂O₃ to β -Ga₂O₃ transition are complex, involving both displacive and constructive transformations that likely played a secondary role in the disruption of the microstructure. They are also complex relative to the singular reconstructive transformations and much smaller volume changes that occur in the transitions of $\kappa(\epsilon)$ -Ga₂O₃ and γ -Ga₂O₃ films to β -Ga₂O₃.

Acknowledgments

This material is based upon work supported by the Air Force Office of Scientific Research (Program Manager, Dr. Ali Sayir) under Award No. FA9550-21-1-0360, and by the II-VI Foundation. The use of the Materials Characterization Facility at Carnegie Mellon University was supported by Grant No. MCF-677785. J. T. and K. J. would also like to acknowledge the Neil and Jo Bushnell Fellowship in Engineering for additional support.

Conflict of Interest

The authors have no conflicts to disclose.

Data Availability

The data that support the findings of this study are available from the corresponding author upon reasonable request.

References

- ¹ T. Kato, H. Nishinaka, K. Shimazoe, K. Kanegae, and M. Yoshimoto, “Demonstration of Bixbyite-Structured δ -Ga₂O₃ Thin Films Using β -Fe₂O₃ Buffer Layers by Mist Chemical Vapor Deposition,” *ACS Appl. Electron. Mater.* **5**(3), 1715–1720 (2023).
- ² R. Roy, V.G. Hill, and E.F. Osborn, “Polymorphism of Ga₂O₃ and the system Ga₂O₃—H₂O,” *J. Am. Chem. Soc.* **74**(3), 719–722 (1952).
- ³ K. Yamaguchi, “First principles study on electronic structure of β -Ga₂O₃,” *Solid State Commun.* **131**(12), 739–744 (2004).
- ⁴ Y. Zhang, J. Yan, G. Zhao, and W. Xie, “First-principles study on electronic structure and optical properties of Sn-doped β -Ga₂O₃,” *Phys. B* **405**(18), 3899–3903 (2010).
- ⁵ N. Ueda, H. Hosono, R. Waseda, and H. Kawazoe, “Anisotropy of electrical and optical properties in β -Ga₂O₃ single crystals,” *Appl. Phys. Lett.* **71**, 933–935 (1997).
- ⁶ Z. Guo, A. Verma, X. Wu, F. Sun, A. Hickman, T. Masui, A. Kuramata, M. Higashiwaki, D. Jena, and T. Luo, “Anisotropic thermal conductivity in single crystal β -gallium oxide,” *Appl. Phys. Lett.* **106**(11), 111909 (2015).
- ⁷ D. Shinohara, and S. Fujita, “Heteroepitaxy of corundum-structured α -Ga₂O₃ thin films on α -Al₂O₃ substrates by ultrasonic mist chemical vapor deposition,” *Jpn. J. Appl. Phys.* **47**, 7311–7313 (2008).
- ⁸ A. Segura, L. Artús, R. Cuscó, R. Goldhahn, and M. Feneberg, “Band gap of corundumlike α -Ga₂O₃ determined by absorption and ellipsometry,” *Phys. Rev. Mater.* **1**(2), 024604 (2017).
- ⁹ Y. Oshima, and E. Ahmadi, “Progress and challenges in the development of ultra-wide bandgap semiconductor α -Ga₂O₃ toward realizing power device applications,” *Appl. Phys. Lett.* **121**(26), 260501 (2022).
- ¹⁰ M. Oda, R. Tokuda, H. Kambara, T. Tanikawa, T. Sasaki, and T. Hitora, “Schottky barrier diodes of corundum-structured gallium oxide showing on-resistance of 0.1m Ω ·cm² grown by MIST EPITAXY®,” *Appl. Phys. Express* **9**(2), 021101 (2016).
- ¹¹ H. Chen, H. Wang, C. Wang, and K. Sheng, “Low Specific On-Resistance and Low Leakage Current β -Ga₂O₃(001) Schottky Barrier Diode through Contact Pre-Treatment,” 2022 IEEE 34th International Symposium on Power Semiconductor Devices 145–148 (2022).
- ¹² K. Konishi, K. Goto, H. Murakami, Y. Kumagai, A. Kuramata, S. Yamakoshi, and M. Higashiwaki, “1-kV vertical Ga₂O₃ field-plated Schottky barrier diodes,” *Appl. Phys. Lett.* **110**(10), 103506 (2017).
- ¹³ S. ichi Kan, S. Takemoto, K. Kaneko, I. Takahashi, M. Sugimoto, T. Shinohe, and S. Fujita, “Electrical properties of α -Ir₂O₃/ α -Ga₂O₃ pn heterojunction diode and band alignment of the heterostructure,” *Appl. Phys. Lett.* **113**(21), 212104 (2018).

- ¹⁴ K. Kaneko, Y. Masuda, S.I. Kan, I. Takahashi, Y. Kato, T. Shinohe, and S. Fujita, “Ultra-wide bandgap corundum-structured p-type α -(Ir,Ga)₂O₃ alloys for α -Ga₂O₃ electronics,” *Appl. Phys. Lett.* **118**(10), 102104 (2021).
- ¹⁵ S. Fujita, and K. Kaneko, “Epitaxial growth of corundum-structured wide band gap III-oxide semiconductor thin films,” *J. Cryst. Growth* **401**, 588–592 (2014).
- ¹⁶ F. He, K. Jiang, Y. Choi, B.L. Aronson, S. Shetty, J. Tang, B. Liu, Y. Liu, K.P. Kelley, G.B. Rayner, R.F. Davis, L.M. Porter, and S. Trolier-McKinstry, “High field dielectric response in κ -Ga₂O₃ films,” *J. Appl. Phys.* **134**(20), 204101 (2023).
- ¹⁷ S. Yusa, D. Oka, and T. Fukumura, “High- κ dielectric ϵ -Ga₂O₃ stabilized in a transparent heteroepitaxial structure grown by mist CVD at atmospheric pressure,” *CrystEngComm* **22**, 381–385 (2020).
- ¹⁸ K. Shimada, “First-principles study of crystal structure, elastic stiffness constants, piezoelectric constants, and spontaneous polarization of orthorhombic Pna2₁-M₂O₃ (M = Al, Ga, In, Sc, Y),” *Mater. Res. Express* **5**(3), 036502 (2018).
- ¹⁹ M.B. Maccioni, and V. Fiorentini, “Phase diagram and polarization of stable phases of (Ga_{1-x}In_x)₂O₃,” *Appl. Phys. Express* **9**(4), 041102 (2016).
- ²⁰ V. Devthade, A. Gupta, and S.S. Umare, “Graphitic carbon nitride- γ -gallium oxide (GCN- γ -Ga₂O₃) nanohybrid photocatalyst for dinitrogen fixation and pollutant decomposition,” *ACS Appl. Nano Mater.* **1**(10), 5581–5588 (2018).
- ²¹ T. Wang, S.S. Farvid, M. Abulikemu, and P. V. Radovanovic, “Size-tunable phosphorescence in colloidal metastable γ -Ga₂O₃ nanocrystals,” *J. Am. Chem. Soc.* **132**(27), 9250–9252 (2010).
- ²² H. Hayashi, R. Huang, H. Ikeno, F. Oba, S. Yoshioka, I. Tanaka, and S. Sonoda, “Room temperature ferromagnetism in Mn-doped γ -Ga₂O₃ with spinel structure,” *Appl. Phys. Lett.* **89**(18), 181903 (2006).
- ²³ Z. Wen, K. Khan, K. Sun, R. Wellen, Y. Oshima, and E. Ahmadi, “Thermal stability of HVPE-grown (0001) α -Ga₂O₃ on sapphire template under vacuum and atmospheric environments,” *J. Vac. Sci. Technol. A* **41**(4), 043403 (2023).
- ²⁴ R. Jinno, K. Kaneko, and S. Fujita, “Thermal stability of α -Ga₂O₃ films grown on c-plane sapphire substrates via mist-CVD,” *AIP Adv.* **10**(11), 115013 (2020).
- ²⁵ J.P. McCandless, C.S. Chang, K. Nomoto, J. Casamento, V. Protasenko, P. Vogt, D. Rowe, K. Gann, S.T. Ho, W. Li, R. Jinno, Y. Cho, A.J. Green, K.D. Chabak, D.G. Schlom, M.O. Thompson, D.A. Muller, H.G. Xing, and D. Jena, “Thermal stability of epitaxial α -Ga₂O₃ and (Al,Ga)₂O₃ layers on m-plane sapphire,” *Appl. Phys. Lett.* **119**(6), 062102 (2021).
- ²⁶ R. Fornari, M. Pavesi, V. Montedoro, D. Klimm, F. Mezzadri, I. Cora, B. Pécz, F. Boschi, A. Parisini, A. Baraldi, C. Ferrari, E. Gombia, and M. Bosi, “Thermal stability of ϵ -Ga₂O₃ polymorph,” *Acta Mater.* **140**, 411–416 (2017)

- ²⁷ S.D. Lee, K. Akaiwa, and S. Fujita, “Thermal stability of single crystalline alpha gallium oxide films on sapphire substrates,” *Phys. Status Solidi* **10**(11), 1592–1595 (2013).
- ²⁸ K. Jiang, J. Tang, M.J. Cabral, A. Park, L. Gu, R.F. Davis, and L.M. Porter, “Layered phase composition and microstructure of κ -Ga₂O₃-dominant heteroepitaxial films grown via MOCVD,” *J. Appl. Phys.* **131**(5), 055305 (2022).
- ²⁹ J. Tang, K. Jiang, C. Xu, M.J. Cabral, K. Xiao, L.M. Porter, and R.F. Davis, “Atomic-scale investigation of γ -Ga₂O₃ deposited on MgAl₂O₄ and its relationship with β -Ga₂O₃,” *APL Mater.* **12**(1), 011109 (2024).
- ³⁰ Y. Zhuo, Z. Chen, W. Tu, X. Ma, Y. Pei, and G. Wang, “ β -Ga₂O₃ versus ε -Ga₂O₃ : Control of the crystal phase composition of gallium oxide thin film prepared by metal-organic chemical vapor deposition,” *Appl. Surf. Sci.* **420**, 802–807 (2017).
- ³¹ A. Hassa, C. Wouters, M. Kneiß, D. Splith, C. Sturm, H. V. Wenckstern, M. Albrecht, M. Lorenz and M. Grundmann “Control of phase formation of (Al_xGa_{1-x})₂O₃ thin films on c-plane Al₂O₃,” *J. Phys. D: Appl. Phys.* **53**, 485105 (2020).
- ³² W. Xu, Y. Li, B. Li, X. Xiu, H. Zhao, Z. Xie, T. Tao, P. Chen, B. Liu, R. Zhang, and Y. Zheng, “(3 $\bar{1}$ 0)-Oriented β -Ga₂O₃ grown on (0001) sapphire by halide vapor phase epitaxy: growth and structural characterizations,” *CrystEngComm* **25**, 6044–6049 (2023).
- ³³ J. Tang, K. Jiang, S.D. House, C. Xu, K. Xiao, L.M. Porter, and R.F. Davis, “Mg and Al-induced phase transformation and stabilization of Ga₂O₃-based γ -phase spinels,” *Appl. Phys. Lett.* **123**(1), 012103 (2023).
- ³⁴ K. Jiang, J. Tang, C. Xu, K. Xiao, R.F. Davis, and L.M. Porter, “Evolution of β -Ga₂O₃ to γ -Ga₂O₃ solid-solution epitaxial films after high-temperature annealing,” *J. Vac. Sci. Technol. A* **41**(6), 062702 (2023).
- ³⁵ P.Y. Hou, A.P. Paulikas, and B.W. Veal, “Growth strains and stress relaxation in alumina scales during high temperature oxidation,” *Mater. Sci. Forum* **461**, 671–680 (2004).
- ³⁶ Y. Huang, X. Peng, and X.Q. Chen, “The mechanism of θ - to α -Al₂O₃ phase transformation,” *J. Alloys Compd.* **863**, 158666 (2021).
- ³⁷ S.C. Zhu, S.H. Guan, and Z.P. Liu, “Mechanism and microstructures in Ga₂O₃ pseudomartensitic solid phase transition,” *Phys. Chem. Chem. Phys.* **18**, 18563–18574 (2016).
- ³⁸ S.H. Cai, S.N. Rashkeev, S.T. Pantelides, and K. Sohlberg, “Atomic Scale Mechanism of the Transformation of γ -Alumina to θ -Alumina,” *Phys. Rev. Lett.* **89**(23), 235501 (2002).
- ³⁹ M. Marezuo, and J.P. Remeika, “Bond Lengths in the α -Ga₂O₃ Structure and the High-Pressure Phase of Ga_{2-x}Fe_xO₃,” *J. Chem. Phys.* **46**(5), 1862–1865 (1967).
- ⁴⁰ L.J. Eckert, and R.C. Bradt, “Thermal Expansion of Alpha Ga₂O₃,” *J. Am. Ceram. Soc.* **56**(4), 229–230 (1973).

- ⁴¹ H.Y. Playford, A.C. Hannon, E.R. Barney, and R.I. Walton, “Structures of uncharacterised polymorphs of gallium oxide from total neutron diffraction,” *Chem. Eur. J.* **19**(8), 2803–2813 (2013).
- ⁴² I. Cora, F. Mezzadri, F. Boschi, M. Bosi, M. Čaplovičová, G. Calestani, I. Dódoný, B. Pécz, and R. Fornari, “The real structure of ϵ -Ga₂O₃ and its relation to κ -phase,” *CrystEngComm* **19**, 1509–1516 (2017).
- ⁴³ M. Zinkevich, F.M. Morales, H. Nitsche, M. Ahrens, M. Rühle, and F. Aldinger, “Microstructural and thermodynamic study of γ -Ga₂O₃,” *Z. Metallkunde* **95**, 756–762 (2004).
- ⁴⁴ H. Wang, Y. He, W. Chen, Y.W. Zeng, K. Stahl, T. Kikegawa, and J.Z. Jiang, “High-pressure behavior of β -Ga₂O₃ nanocrystals,” *J. Appl. Phys.* **107**(3), 033520 (2010).
- ⁴⁵ F. Orlandi, F. Mezzadri, G. Calestani, F. Boschi, and R. Fornari, “Thermal expansion coefficients of β -Ga₂O₃ single crystals,” *Appl. Phys. Express* **8**(11), 111101 (2015).